(CHE-8023704) and the Dow Chemical Company Foundation for support of this work. Also, one of us (C.J.C.) thanks Phillips Petroleum for Fellowship Support.

Registry No. CH_3NO_2, 75-52-5; CH_3ONO, 624-91-9; $C_2H_5NO_2$, 79-24-3; $C_3H_7NO_2$, 108-03-2; 1-$C_4H_9NO_2$, 627-05-4; 1-C_4H_9ONO, 544-16-1; 2-$C_3H_7NO_2$, 79-46-9; 2-$C_4H_9NO_2$, 600-24-8; 2-$CH_3CCH_3NO_2CH_3$, 594-70-7; Co^+, 16610-75-6; $CoCO^+$, 28963-35-1; $Co(CO)_2^+$, 28963-34-0; $CoNO^+$, 87616-10-2; $CoCONO^+$, 61816-95-3; $Co(CO)_2NO^+$, 61816-96-4; $Co(CO)_3NO^+$, 52309-13-4.

Ion–Solvent Molecule Interactions in the Gas Phase. The Potassium Ion and Me_2SO, DMA, DMF, and Acetone

Jan Sunner and Paul Kebarle*

Contribution from the Chemistry Department, University of Alberta, Edmonton, Alberta, Canada T6G 2G2. *Received January 23, 1984*

Abstract: Measurements of the gas-phase equilibria $K^+(L)_{n-1} + L = K^+(L)_n$ where K^+ is the potassium ion and L = dimethyl sulfoxide, *N*,*N*-dimethylacetamide, *N*,*N*-dimethylformamide, and acetone with a high-pressure mass spectrometer lead to the corresponding thermomechemical data $\Delta H^\circ_{n-1,n}$, $\Delta G^\circ_{n-1,n}$, and $\Delta S^\circ_{n-1,n}$. The observed stability order of the 1:1 complexes K^+L is the following: Me_2SO (25), DMA (24), DMF (23), $MeOC_2H_4OMe$ (23), $NH_2C_2H_4NH_2$ (19), Me_2CO (19), MeCN (18), $C_6H_5NH_2$ (16), Et_2O (15), pyridine (15), Me_2O (13), Me_3N (13), $MeNH_2$ (13), C_6H_6 (12), NH_3 (12), H_2O (11), where the numbers give the value for $-\Delta G^\circ_{0,1}$ in kcal/mol. Ab initio (4–31G) calculations were performed for the complex K^+Me_2SO. These show that the bonding is largely electrostatic. The major contribution to this bonding is due to the large S–O bond dipole. K^+ lines up with the S–O bond (dipole) in the most stable structure. The higher solvation $(n-1,n)$ steps for Me_2SO, DMA, and DMF are quite similar. These compounds form a much more strongly bonded inner shell with K^+ than H_2O; however, the solvation of the inner-shell cluster $K^+(L)_i$ in these solvents is much less favorable than that for $K^+(H_2O)_i$ in water. This compensating effect leads to only slightly higher single-ion solvation K^+ energies in Me_2SO, DMA, and DMF than in H_2O. The gas-phase equilibria measurements for DMA and DMF led to somewhat curved van't Hoff plots for the higher $(n-1,n)$ equilibria. A theoretical analysis shows that this is probably due to unimolecular dissociation of the corresponding clusters in the vacuum of the mass analysis system. This effect reduces the accuracy of the data.

Measurements of the gas-phase equilibria 1 and 2 for M^+ = alkali cations and X^- = halide anions and the solvent molecules L = H_2O and acetonitrile were reported earlier from this laboratory.[1-4] Measurements of the equilibrium constants $K_{n-1,n}$ for

$$M^+L_n^{-1} + L = M^+L_n \quad (1)$$

$$X^-L_{n-1} + L = X^-L_n \quad (2)$$

(1) and (2) at different temperatures with a pulsed electron beam high pressure mass spectrometer lead via van't Hoff plots to the corresponding stepwise solvation energies $\Delta H^\circ_{n-1,n}$ and $\Delta G^\circ_{n-1,n}$. These data provide useful insights into the solvation of the above ions in liquid solutions of the solvents.

Dimethyl sulfoxide (Me_2SO), *N*,*N*-dimethylacetamide (DMA), *N*,*N*-dimethylformamide (DMF), and acetone are important dipolar aprotic solvents much used in laboratory and industrial synthetic practice. The study of these solvents represents a natural extension of our previous work. The $\Delta G^\circ_{0,1}$ and the $\Delta H^\circ_{0,1}$ energies represent the binding energies in the 1:1 complexes between the ion K^+ and the ligand L. Comparison with data for various other ligands measured earlier[5,6] establishes useful Lewis basicity orders in the absence of a solvent. In this respect DMA and DMF are particularly interesting since they contain elements of peptide-type bonding which is of interest in biophysical chemistry[7] and design of ion-selective electrodes.[8]

The present paper deals only with the results for positive ions. The companion paper[9] which gives results for the negative halide ions deals also with the relative solvation of positive and negative ions in protic and aprotic solvents and the synthetic utility of dipolar aprotic solvents for reactions involving negative ions.

Experimental Section

Apparatus. The apparatus was essentially the same as that used earlier.[3] The potassium ions were produced by thermionic emission from a filament painted with potassium salt. The filament is inside the ion source which contains gas, generally in the 0.5–3-torr range. The gas may be the neat solvent vapor or a mixture of a major, buffer gas (CH_4) containing a small fraction of the solvent vapor. The ions drift under the influence of electric fields into the field-free reaction chamber. At the bottom of the reaction chamber there is a narrow slit ~ 15 μm by 1 mm through which gas and ions escape into the evacuated mass analysis region. The ions are separated with a magnetic field and detected with an ion-counting system.

Results and Effects due to Unimolecular Decomposition of Ions. Equilibrium constants were determined from expression 3 where I_n are the detected counts/time of ions, K^+L_n, and P_L is the known partial pressure of the solvent vapor. The equilibrium constants were measured

$$K_{n-1,n} = \frac{I_n}{I_{n-1}} P_L \quad (3)$$

at different constant temperatures. For any given temperature, measurements at different ligand pressures were performed. Typically the pressure ratio of CH_4-to-ligand vapor was equal to 10, and the pressure of the ligand was changed from 0.05 to 0.3 torr. At very low ligand concentrations the observed $K_{n-1,n}$ tended to decrease, particularly for low *n* cluster equilibria. In special experiments the K^+ supply to the reaction chamber was pulsed, so that the residence time of the ions could be determined. These experiments showed that the low-pressure falloff of the equilibrium constants was due to slow kinetics in the approach to equilibrium. Selecting only ions with long residence time one observed no falloff for $K_{n-1,n}$ at low P_L. Typical results for the pulsed and unpulsed experiments are given in Figure 1. A gradual falloff of *K* with an

(1) Dzidic, I.; Kebarle, P. *J. Phys. Chem.* **1970**, *74*, 1466.
(2) Arshadi, M.; Yamdagni, R.; Kebarle, P. *J. Phys. Chem.* **1970**, *74*, 1975.
(3) Davidson, W. R.; Kebarle, P. *J. Am. Chem. Soc.* **1976**, *98*, 6125.
(4) Yamdagni, R.; Kebarle, P. *J. Am. Chem. Soc.* **1971**, *94*, 2940.
(5) Davidson, W. R.; Kebarle, P. *J. Am. Chem. Soc.* **1976**, *98*, 6133.
(6) Kebarle, P. *Annu. Rev. Phys. Chem.* **1977**, *28*, 445.
(7) (a) Rao, C. N. R. In "Metal-Ligand Interactions in Organic Chemistry and Biochemistry"; Pullman, B., Goldblum, N., Eds.; B. Reidel Publishing: Holand, **1977**. (b) Balasubramanian, D.; Mishra, B. C., ref 7a. (c) Noelken, M. E. *Biochemistry*, **1970**, *9*, 4122. Lothan, N. *J. Phys. Chem.* **1973**, *77*, 242. (d) Truter, M. R. "Structure and Bonding"; Dunitz, J. D., et al., Eds.; Springer: New York, 1973; Vol. 16.
(8) Corongiu, G.; Clementi, E.; Pretch, E.; Simon, W. *J. Chem. Phys.* **1979**, *70*, 1266.
(9) Magnera, T. L.; Caldwell, G.; Sunner, G.; Ikuta, J.; Kebarle, P. *J. Am. Chem. Soc.*, following paper in this issue.

0002-7863/84/1506-6135$01.50/0

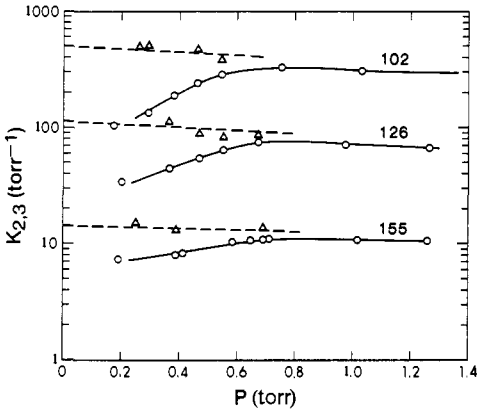

Figure 1. Dependence of the experimental equilibrium constant on pressure in the reaction chamber. Equilibrium measured: $K^+(DMA)_2 + DMA = K^+(DMA)_3$. Numbers given beside plots correspond to temperature (°C). Pressure is total pressure. Mixture used $P_{DMA}/P_{tot} = 1.4 \times 10^{-2}$; the major gas is methane. (Δ) Experiments were K^+ was pulsed and only $K^+(DMA)_n$ ions with long reaction chamber residence times were used for evaluation of the equilibrium constant. These data show that fall-off of the unpulsed (O) data equilibrium constant at low pressure is due to slow kinetic approach to equilibrium at these pressures.

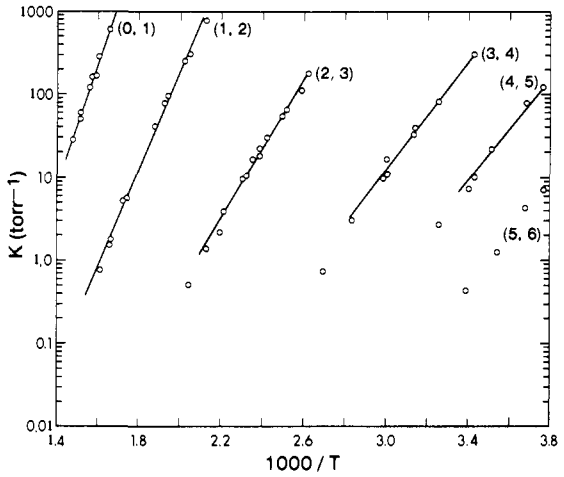

Figure 2. van't Hoff plot for $(n-1,n)$ reactions: $K^+(Me_2SO)_{n-1} + Me_2SO = K^+(Me_2SO)_n$.

increase of P_L was also observed, particularly for DMA and DMF. This effect will be discussed further on in this section. van't Hoff plots for the equilibrium constants observed with L = Me_2SO, DMA, DMF, and acetone are shown in Figures 2–5. Examining these results one finds that the DMA and DMF plots show noticeable curvature while those for acetone and Me_2SO are close to being straight lines. The curvature in the DMA and DMF plots generally increases with an increase of the cluster size (see Figure 5). Good straight lines have been observed for practically all compounds investigated in previous work.[6] The curvature of the DMA and DMF plots prompted us to undertake an analysis of the measurement conditions. Some of the results from this analysis have already been published.[10a] It appears that the problem is due to dissociation of the clusters in the vacuum of the mass analysis system. The dissociation may be unimolecular[10a] or collision induced.[10a,11] For systems like DMA and DMF, the unimolecular decomposition is the more serious source of error. Unimolecular decomposition occurs for clusters n which when leaving the high-pressure ion source have an internal energy E_n which is higher than the cluster-dissociation energy $E^\circ_n \approx -\Delta H^\circ_{n-1,n}$. The frequencies for the normal vibrations (including internal rotations) of the cluster K^+L_n must be known; in practice they are estimated. From these frequencies, assuming a Maxwell Boltzmann distribution at the temperature of the reaction chamber, one can calculate the energy distribution probability function $P_n(E)$ of the clusters K^+L_n

(10) (a) Sunner, J.; Kebarle, P. *J. Phys. Chem.* **1981**, *85*, 327. Sunner, J.; Magnera, T. F.; Kebarle, P. *Can. J. Chem.* **1981**, *59*, 1787. (b) Details concerning the calculations, i.e., frequencies used for the clusters and the transition states for the dissociation $K^+(DMA)_n \rightarrow K^+(DMA)_n^{-1} + DMA$, are available upon request from the author P.K. The frequencies were obtained from force field calculations involving $K^+(DMA)_n$. The force field was based on electrostatic calculations as described by Sunner.[10a] These "first choice" frequencies were used in the RRKM calculations. Better agreement with the experimental results could have been obtained by changing the above frequencies; however, this was not done.

(11) Lau, Y. K.; Ikuta, S.; Kebarle, P. *J. Am. Chem. Soc.* **1982**, *104*, 1462.

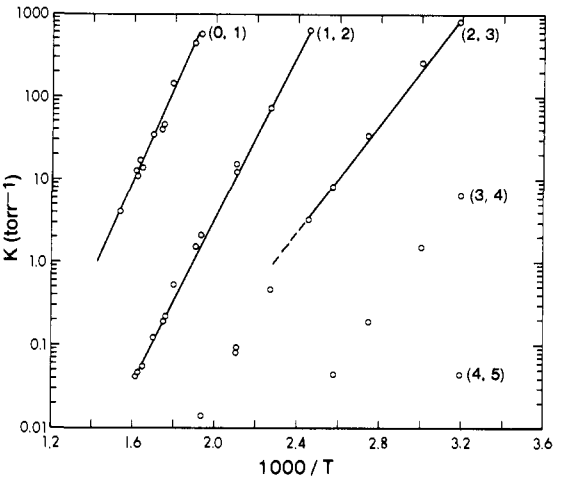

Figure 3. van't Hoff plots for reactions $(n-1,n)$: $K^+(Me_2CO)_{n-1} + Me_2CO = K^+(Me_2CO)_n$. Data lead to noticeable curvature for the (2,3) plot.

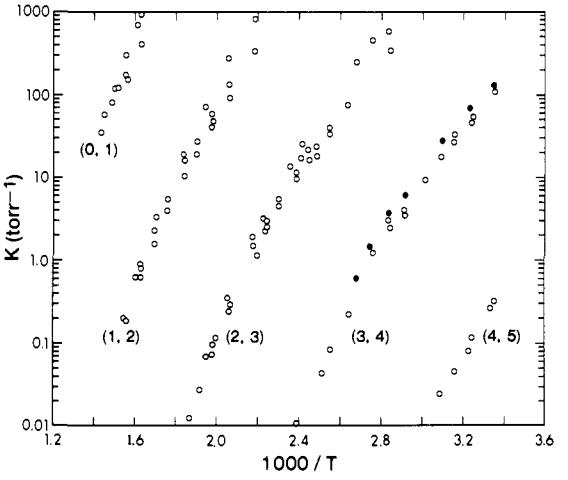

Figure 4. van't Hoff plot for reactions $(n-1,n)$: $K^+(DMA)_{n-1} + DMA = K^+(DMA)_n$. Experimental points include equilibrium determinations obtained under a variety of conditions; in the (3,4) plot the equlibrium constants obtained from extrapolation to zero DMA pressure are shown separately (●). Noticeable curvature is observed in the (2,3) and (3,4) plots.

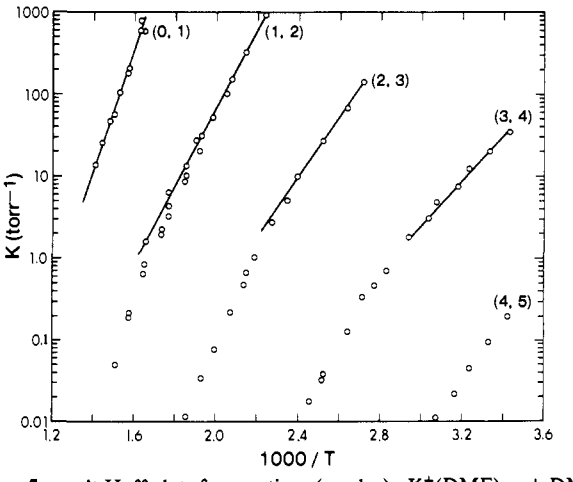

Figure 5. van't Hoff plots for reactions $(n-1,n)$: $K^+(DMF)_{n-1} + DMF = K^+(DMF)_n$. Curvature is observed for the (1,2) to (3,4) plots. Solid lines indicate the region from which data for Table I were taken.

Table I. Thermochemical Data from van't Hoff Plots for Reactions $K^+L_{n-1} + L = K^+L_n$ where L = Me_2SO, DMA, DMF, and Acetone[a]

reaction	$-\Delta H°$, kcal/mol					$-\Delta S°$, cal/(deg mol)					$-\Delta G°_{300}$, kcal/mol				
$n-1,n$	Me_2SO	DMA[b]	DMF[b]	Me_2CO[b]	H_2O[d]	Me_2SO	DMA[b]	DMF[b]	Me_2CO[b]	H_2O[d]	Me_2SO	DMA[b]	DMF[b]	Me_2CO[b]	H_2O[d]
0,1	35 ± 3	31	31	26	17.9	31	23 ± 6	26	24	22	25 ± 3	24 ± 2	23	19	11.4
1,2	29 ± 2	24	21	21	16.1	34	24 ± 4	20	26	22	19 ± 1	16.5 ± 1	15	13	8.9
2,3	20 ± 1	18	15	16	13.2	28	24 ± 4	18	24	24	11 ± 1	11 ± 1	9.6	9	6.3
3,4	16 ± 1		13	*c*	11.8	30		24	*c*	23	7 ± 1		5.8	*c*	4.4
4,5	15.8 ± 1				10.7	37				25	5 ± 1				3.2
5,6	15.5 ± 1				10.0	40				26	3 ± 1				2.3

[a] From van't Hoff plots Figures 1–4. [b] The van't Hoff plots for all $n-1,n$ reactions except (0,1) for this ligand show some curvature. As explained in the text, the low-temperature region of the plots is believed to be more reliable because it is less affected by decomposition of the clusters during mass analysis. The ΔH, ΔS, and ΔG values given in the table were taken from the low-temperature region. [c] The low-temperature region of van't Hoff plot was not reached (see Figures 2–5). [d] From Dzidic.[1]

and the fraction of clusters f^n that has internal energy above $E°_n$. Then, RRKM theory is used[10a] to calculate the rate constants $k_n(E)$. The ion-flight times (~10 to 20 μs) are relatively long so that most of the clusters excited above $E°_n$ dedcompose. Those that decompose very rapidly may be detected as K^+L_{n-1}, while the slower ones may be detected as metastable ions. The previously published analysis[10a] dealt with the system $K^+(H_2O)_n$ for which curvature in the van't Hoff plots was not really noticeable. However, that system because of the simplicity of the ligands (H_2O) was easier to model mathematically. Calculations of the same type were performed also for DMA. Because of the greater complexity of the DMA molecule, more assumptions had to be made which led to somewhat cruder modeling. Therefore, we will not give here the full details of the calculations[10b] but only describe some of the pertinent results. Shown in Figure 6 is a comparison between the experimental van't Hoff plots and the calculations. Since the theory predicted that the experimental plots should be closest to the true values when P_{DMA} approaches zero and when the temperature is as low as possible, the low-temperature region for each $(n-1,n)$ plot obtained from experimental $K_{n-1,n}$ extrapolated to $P \rightarrow 0$ (see Figure 1) were taken as the "true" results and used to construct "true" van't Hoff lines over an extended temperature range. The extrapolations to $P = 0$ based on the pulsed experiments at low P or the unpulsed experiments at higher P gave similar results (see Figure 1). The pulsed experiments lead to much lower intensities which makes the measurements more difficult. Therefore, the majority of the results were obtained from the continuous experiments.

The effect that unimolecular dissociation would have in modifying the assumed "true" values was then calculated for $P_{DMA} \rightarrow 0$ and P_{DMA} = 0.2 torr. The theoretical lines containing the predicted effect of the decomposition are shown in Figure 6. For the (0,1) equilibrium the adulteration by decomposition is small. For the (1,2) equilibrium, there is fair agreement between the deviation from linearity observed experimentally at high temperatures and the deviation due to decomposition predicted by the calculation.

For the (2,3) equilibria the deviation from linearity of the experimental results is large. The experimental results at zero pressure are fairly well followed by the predicted results for zero pressure although the predicted deviation at high T are larger. The agreement between the experimental and predicted results at high pressure is much less good, but on the whole, qualitatively, the two predicted curves are similar in appearance to the experimental ones. The calculations also predict a gradual decrease of the observed $K_{n-1,n}$ at constant temperature and increasing pressure of DMA. This predicted decrease was of similar magnitude as that experimentally observed. Thus, the theoretical analysis provides a qualitative proof that unimolecular decomposition is the cause of the observed deviations; however, the effect cannot be considered as completely proven.

The $K^+(DMA)_n$ frequencies[10b] were also used to examine the change in $\Delta H°_{n-1,n}$ with temperature. These calculations showed that the curvature in the experimental van't Hoff plots is very much larger than the almost negligible curvature due to $\int \Delta c_p \, dT$ contributions to $\Delta H°_{n-1,n}$.

For the (1,2), (2,3), and (3,4) DMA equilibria we have used the low-temperature regions of the experimental plots, from $P \rightarrow 0$ pressure, to obtain the corresponding $\Delta H°_{n-1,n}$, $\Delta G°_{n-1,n}$, and $\Delta S°_{n-1,n}$. These data are given in Table I. Evidently, the confidence in these values decreases as n increases. While a detailed analysis was not made for DMF, the situation for this compound should be similar and a similar procedure was followed to obtain the data given in Table I. For acetone the observed curvature is small; nevertheless, only the lower temperature region for (1,2) and (2,3) plots was used. The Me_2SO plots which show least curvature were used "as they were".

Dscussion

A. The 0,1 Interaction Energies, i.e., the 1:1 Complexes: K^+L. A very direct comparison of the stabilities of K^+L complexes is provided by Figure 7 which gives the van't Hoff plots of the equilibrium constants $K_{0,1}$. Some earlier determinations of other compounds are included for comparison. The higher the position of the line in the figure, the higher the thermodynamic stability of the complex in the temperature range of the experimental determinations. Table II gives numerical data for the energies and entropies for all the K^+L complexes for which gas-phase measurements have been performed.[1,3,5,12,13] The order of the van't Hoff plots observed in Figure 7 is DMA ≈ DMF ≈ Me_2SO > 1,2-dimethoxyethane > 1,2-diaminoethane > MeCN > Me_2CO ≫ Et_2O > $PrNH_2$ > Me_2O > NH_3 > H_2O. This order is very similar to the order in Table II where the compounds have been arranged in order of decreasing $-\Delta H°_{0,1}$ values. This is a consequence of the rather similar $\Delta S°_{0,1}$ changes (see Table II). The strong bonding of Me_2SO, DMA, and DMF to K^+ could have been expected because of the very high dipole moment of these compounds; however, it is somewhat surprising that these compounds bond more strongly even than the bidentate ligands 1,2-dimethoxyethane and 1,2-diaminoethane.

The donor numbers of Gutman[14] corresponding to ΔH (kcal/mol) for the reaction $SbCl_5 + L = SbCl_5L$ in 1,2-dichloroethane are also given in Table II. The donor numbers for

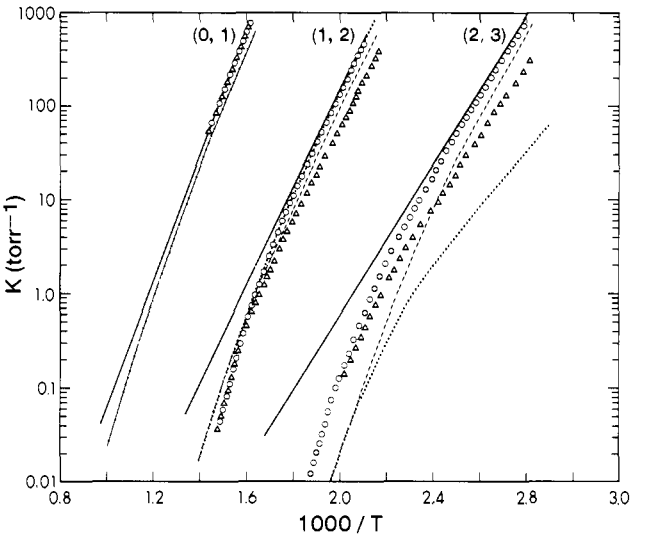

Figure 6. Results from theoretical analysis of the unimolecular decomposition effect on measured equilibria $K^+(DMA)_{n-1} + DMA = K^+(DMA)_n$. (—) Assumed true van't Hoff lines; (○) van't Hoff lines obtained from experiment where DMA pressure approaches zero; (△) experiment, P_{DMA} = 0.2 torr; (- - -) van't Hoff lines predicted from calculation for zero DMA pressure; (···) van't Hoff lines predicted by calculation for P_{DMA} = 0.2 torr. Comparison between assumed true van't Hoff lines and calculated lines shows the predicted effect of unimolecular decomposition. Although the calculated effect of unimolecular decomposition is larger than that observed by experiment, calculation reproduces qualitively the features of the experimental observations.

(12) Davidson, W. R.; Kebarle, P. *Can. J. Chem.* **1976**, *54*, 2594.
(13) Sunner, J.; Nishizawa, K.; Kebarle, P. *J. Phys. Chem.* **1981**, *85*, 1814.
(14) Mayer, U.; Gutmann, V.; Berger, W.; Monatsheffe F. *Chemie* **1975**, *166*, 1235.

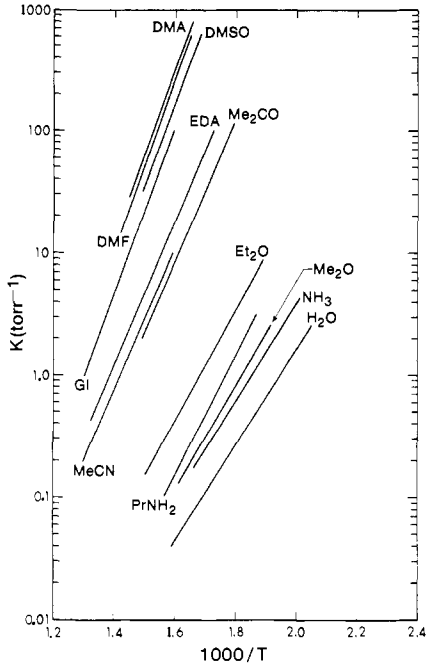

Figure 7. van't Hoff plots for $K^+ + L = K^+L$ for different ligands L. The stability of the K^+L complex decreases from the northwest corner to the southeast. DMA, DMF, and Me_2SO form the most stable complexes. These are even more stable than the bidentate ligand Gl(1,2-dimethoxyethane) and EDA(1,2-diaminoethane) complexes.

Table II. Thermochemistry of Complexes K^+L[a]

L	$\Delta H_{0,1}$	$\Delta G°_{0,1}$	D[b]	$\Delta S°_{0,1}$	dipole moment[c]	ref[d]
Me_2SO	35	25	29.8	31	3.9	this work
DMA	31	24	27.8	23	3.81	this work
DMF	31	23	26.6	26	3.9	this work
$(MeOCH_2)_2$	31	23		27		12
$(NH_2CH_2)_2$	26	19		22		12
Me_2CO	26	19	17	24	2.88	this work
MeCN	24	18	14.1	22	3.9	3
aniline	23	16		24		5
Et_2O	22	15	19.2	25	1.25	5
n-$PrNH_2$	22	14		26	1.18	5
pyridine	21	15	33.1	17	2.2	5
Me_2O	21	13		25	1.3	5
Me_3N	20	13		23	0.63	5
Me_2NH	20	13		21	1.0	5
$MeNH_2$	19	13		22	1.29	5
benzene	19	12	0.1	24		13
NH_3	18	12		20	1.47	5
H_2O	17	11	18	20	1.8	1

[a] ΔH and ΔG (300 K) in kcal/mol, S in eu, standard state 1 atm. [b] D is the donor number, Gutman.[14] [c] Dipole moment in Debye units. [d] References relate to the source of ΔH, ΔG, and ΔS values.

Me_2SO, DMA, DMF, and acetone appear almost proportional to the $-\Delta H°_{0,1}$ (respectively $-\Delta G°_{0,1}$) values. A fair correlation exists also for most of the other ligands; however, there are also some glaring differences. Thus, pyridine which bonds relatively weakly to K^+ has a donor number which is higher that that for Me_2SO, DMF, and DMA! On the other hand, benzene has a much stronger interaction with K^+ than expected on the basis of its very low donor number. The low donor number for benzene is probably due largely to its favorable solvation by dichloroethane which reduces its tendency to react with $SbCl_5$, but the reason for the very high donor number of pyridine is not clear.

Clementi et al.[8] have made theoretical studies of the complexing of Na^+ with N,N-methylethylacetamide. They find that in the most stable structure the sodium ion is in line with the C=O bond axis. The same alignment almost certainly occurs also in the K^+DMA complex. Thus in DMA, DMF, and acetone the major interaction occurs with the carbonyl oxygen and the carbonyl bond dipole. The much stronger bonding for the amides as compared

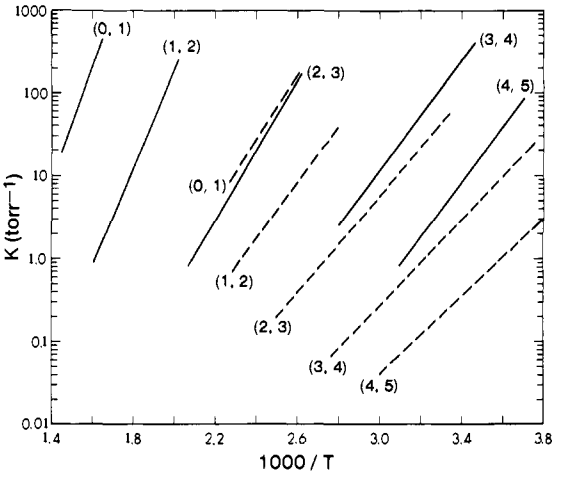

Figure 8. Comparison of stabilities of $K^+(Me_2SO)_n$ (—) and $K^+(H_2O)_n$ (- - -). The Me_2SO complexes are very much more stable than those of H_2O; however, stability differences decrease with an increase in n. This is directly indicated by the relatively narrow spacings between $(n-1,n)$ plots for H_2O.

to acetone is obviously due to the much higher electron-donating ability of the amino group (Me_2N) relative to Me. The electron donation from the amino group is expected to be mostly π-type dontion from the lone pair on the nitrogen. Evidence for this electron pair shift is provided by the increased hindrance to internal rotation around the C–N bond which occurs on complexing of amide with a positive ion.[15]

Theoretical calculations for $K^+(Me_2SO)$ were performed in our laboratory using the 4-31G basis set for the atoms in Me_2SO[16] and the basis set of Huzinaga[17] for the potassium ion. Alignment of K^+ with the S=O bond leads to the most stable structure, shown below.

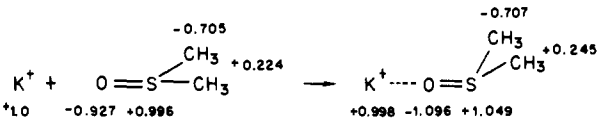

4-31G

$\Delta E_{0,1} = -39.6$ kcal/mol; $r(0\cdots K^+) = 2.45$ Å

The calculated exothermicity of the complex formation $\Delta E_{0,1} = -39.6$ kcal/mol is in fair agreement with the measured $\Delta H_{0,1} = -35 \pm 3$ kcal/mol. The disagreement probably is due to deficiency of the basis sets used and error in the experimental determination. The net atomic charges based on Mulliken electron populations given above predict a very small (0.002) electron transfer from Me_2SO to K^+ on formation of the complex. Thus, the bonding is due mostly to electrostatic interaction, the biggest contribution to which is made by the very large O–S bond dipole. A smaller contribution is due to polarizability, mainly that of the SO group. The polarizability effect is illustrated by the change of the net atomic charges of the O, S, C, and H atoms before and after the complex formation. Additional information on the calculations and the bonding in K^+Me_2SO is given in the companion paper[9] in connection with a comparison of the bonding for the isoelectronic ions K^+ and Cl^- with Me_2SO.

B. Sequential Solvation of K^+. The sequential solvation of K^+ by Me_2SO, DMF, and DMA, Table I and Figures 1–3, is quite similar, and since the Me_2SO data are the least affected by unimolecular dissociation and Me_2SO in an important solvent,

(15) Rode, B. M. In "Metal-Ligand Interaction in Organic Chemistry and Biochemistry"; Pullman, B., Goldblum, N., Eds., Reidel Publishing: Dordrecht-Holland/Boston, 1977.

(16) The ab initio MO calculations were performed with HONDO5 and GAUSSIAN 70 programs. King, H.; Dupuis, M.; Rys. J. Nat. Resource Comput. Chem. Software Cat. 1980, Vol. 1 PROG No. QH02 (HONDO5), 1980, Lawrence Berkeley Laboratory, University of California.

(17) Huzinaga, S., Chemistry Department, University of Alberta, Edmonton, Alberta, Canada T6G 2G2.

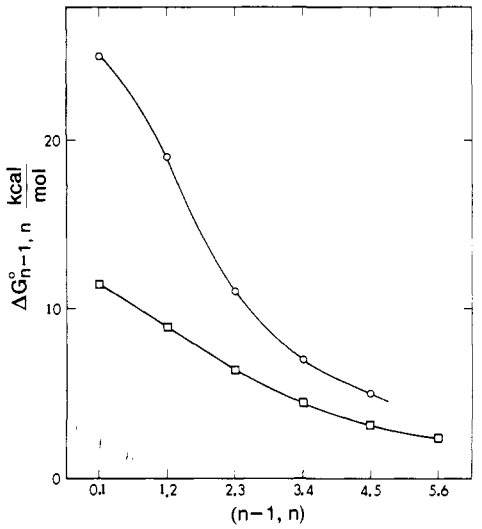

Figure 9. Free energy changes at 300 K for K^+Me_2SO (○) and $K^+(H_2O)$ (□). While Me_2SO interactions are much stronger, they decrease faster such that at $(n-1,n) > (5,6)$ a crossover to stronger H_2O interactions is indicated.

we will base the discussion on the Me_2SO results. A comparison of the solvation of K^+ by water and Me_2SO is of special interest. Previously measured values for the hydration of K^+ are included in Table I. A very direct comparison of the two solvents is obtained by examining the van't Hoff plots for the two solvents shown in Figure 8. It is immediately clear that not only the 0,1 interaction but also the subsequent steps up to the highest measured values for H_2O are very much weaker than those for Me_2SO. This is true for both the $-\Delta H^{\circ}_{n-1,n}$ and the $-\Delta G^{\circ}_{n-1,n}$ values. Another direct observation that can be made from the van't Hoff plots in Figure 8 is the closer spacing of the individual van't Hoff lines for H_2O when compared to those for Me_2SO. This means that the falloff in bonding (free energy) with increasing cluster size is much slower for water than for Me_2SO. A plot of $-\Delta G^{\circ}_{n-1,n}$ for K^+Me_2SO and K^+H_2O is shown in Figure 9. The $-\Delta G^{\circ}_{n-1,n}$ values for Me_2SO are much larger for low n; however, due to more rapid falloff with n, the values become nearly equal to the H_2O results at (5,6). The observed more rapid fall off for Me_2SO is probably due to the larger repulsion between the Me_2SO molecules. The Me_2SO dipole is much larger than that for H_2O (Table II) so that a higher intermolecular dipole repulsion for Me_2SO molecules is to be expected.

The gas-phase cluster thermochemical data often do not indicate a sharp transition between inner and outer shell. In the earlier work on K^+ and acetonitrile[3] a noticeable discontinuity in the increasing spacing between the MeCN van't Hoff plots between (3,4) and (4,5) indicated a greater decrease of stability after the fourth MeCN molecule. On the other hand, the K^+H_2O data did not have a noticeable discontinuity. The K^+Me_2SO data (van't Hoff plots in Figure 2 and $\Delta G^{\circ}_{n-1,n}$ values in Figure 9) also do not show a noticeable discontinuity within the experimentally observed range. The observed range $n = 1$ to $n \approx 4$–6 can be assumed to correspond to first shell type interactions. As more molecules cluster the interactions will shift to typical "second shell" type. For these clusters one expects the difference between the size of Me_2SO and H_2O to become a prominent feature. The much bigger and longer Me_2SO molecule will force outer-shell molecules to be much farther away from the ion core and lead to weak outer-shell interactions for Me_2SO. Conversely, the small size of the inner-shell $K^+(H_2O)_i$ cluster will lead to significant further solvation by H_2O. This effect would have been directly observable from the gas-phase stepwise solvation energies had data been available up to much larger clusters. An approximate evaluation of the solvation of the inner-shell clusters $K^+(Me_2SO)_i$ and $K^+(H_2O)_i$ in liquid Me_2SO and H_2O, respectively, is possible (see subsequent paper in this issue[9]). This treatment shows that the solvation of the $K^+(Me_2SO)_i$ in Me_2SO is much weaker than that for $K^+(H_2O)_i$ in water. The much stronger inner-shell solvation by Me_2SO, followed by the much weaker subsequent solvation combine to lead to only a slightly stronger single-ion solvation for K^+ in liquid Me_2SO relative to that in liquid water.[9]

Acknowledgment. The K^+Me_2SO 4-31G calculation was performed by Dr. S. Ikuta. This work was supported by the Canadian National Science and Engineering Research Council.